Thermochimica Acta 496 (2009) 110–116

Contents lists available at ScienceDirect

Thermochimica Acta

journal homepage: www.elsevier.com/locate/tca

Structure, morphology and thermal stability of electrochemically obtained Ni–Co deposits

L.D. Rafailović[a], W. Artner[b], G.E. Nauer[b,c], D.M. Minić[d,*]

[a] Physics of Nanostructured Materials, Faculty of Physics, University of Vienna, Boltzmanngasse 5, 1090 Vienna, Austria
[b] Centre of Electrochemical Surface Technology (CEST), Viktor-Kaplan-Straße 2, A-2700 Wr. Neustadt, Austria
[c] Faculty of Chemistry, University of Vienna, Währinger Straße 42, A-1090 Vienna, Austria
[d] Faculty of Physical Chemistry, University of Belgrade, Studentski trg 12, 11000 Belgrade, Serbia

ARTICLE INFO

Article history:
Received 12 May 2009
Received in revised form 11 July 2009
Accepted 14 July 2009
Available online 21 July 2009

Keywords:
Nanostructured materials
Electrochemical deposition
Structure
Morphology
Thermal treatment
Alloy powder
Phase transformation

ABSTRACT

Nanostructured nickel–cobalt alloy powder deposits were obtained electrochemically on Cu substrates in the current density range 40–400 mA cm^{-2}. The influence of the current density and of the Ni^{2+}/Co^{2+} ratio in the bath on the microstructure and phase composition of the Ni–Co deposits was studied by SEM and X-ray diffraction methods. Both the bath composition and the current density strongly influence the deposit growth mechanism as well as the deposit composition, microstructure, grain size and surface morphology. If the concentration ratio in the electrolyte is $Ni^{2+}/Co^{2+} = 4$, the deposit has a cauliflower structure with mean grain size of 13 nm. In contrast, the particles deposited from the electrolyte with $Ni^{2+}/Co^{2+} = 0.25$ show platelet structure with preferred orientations and mean grain size of 20 nm. When electrodeposition was performed at high overpotentials, far from equilibrium conditions, face-centered cubic (FCC) solid solutions of Ni and Co were generated while at low overpotentials, as well as at higher content of cobalt in the electrolyte, hexagonal-close packed (HCP) Co was formed. The structure of nanocrystalline deposits exhibits a strong tendency to structural changes under annealing. DSC of the alloy deposits shows a stepwise process of structural changes in the temperature range from 393 to 823 K. It was found that under annealing, HCP → FCC phase transformation occurs in nanocrystalline deposit obtained from electrolyte with a concentration ratio $Ni^{2+}/Co^{2+} = 0.25$.

1. Introduction

From the earliest papers in the nanostructured material science [1] until now, nanoscaled materials have attracted a lot of attention from scientists all over the world concerning both scientific and technological aspects [2–4]. Many synthesis techniques for the production of nanostructured materials have been developed, for example, inert gas-condensation, ball-milling, severe plastic deformation, chemical vapor deposition and electrochemical deposition [3]. Although electrodeposition is a method that uses well known processes for synthesizing nanocrystalline materials, the properties of the nanocrystalline electrodeposits formed by this method are less well known, especially for tribological application in nanoscale devices such as micro and nanoelectromechanical systems (MEMS and NEMS) [5,6].

Electrodeposited Ni, Co and Ni–Co alloys have become an important component in MEMS [7,8]. Reducing the grain size of electrodeposits to the nanocrystalline regime (i.e. below 100 nm) has recently received considerable interests for MEMS applications. However, a common finding in the thermal stability studies of electrodeposited nanocrystalline Ni is the significantly increased rate of grain growth at relatively low temperatures [7,8]. For example, thermal exposure of 30 min at 693 K is sufficient to completely consume the as-deposited nanocrystalline matrix by abnormal grain growth [8]. However, it is possible to design the starting nanocrystalline microstructure – by alloying with Co [7]. Properties of nanostructured or nanocrystalline materials are significantly affected by the large fraction of atoms that are situated at or near an external interface, i.e. near the surface or near the grain (or heterophase) boundary [9].

The electrodeposition technique has significant advantages compared to other methods for the synthesis of nanocrystalline materials; among the advantages is the easy preparation of materials of high purity exhibiting different structures and morphologies and the possibility of changing the composition and morphology within a broad range, adjusting only the deposition parameters [10,11].

Electrodeposition of Ni–Co powders from defined solutions was established by the work of Calusaru [12]. Almost all metals can be obtained in powder form, but the method for obtaining such

* Corresponding author. Tel.: +381 11 332 2883.
E-mail address: dminic@ffh.bg.ac.rs (D.M. Minić).

0040-6031/$ – see front matter © 2009 Elsevier B.V. All rights reserved.
doi:10.1016/j.tca.2009.07.007

materials will depend on the intended properties and will affect the structure of the materials [12]. The electrolytic powder production method usually yields a product which has the desired chemical composition and high purity and which can be well pressed and sintered as we have shown in previous papers [13–15]. Fine Ni, Co and NiCo alloy powders are required for developing magnetoresistive sensors in thick-film form [16].

The electrodeposition of Co has been studied far less than Ni electrodeposition [17]. Electrolytic Co crystallizes with two structures: HCP, the stable allotropic modification at temperatures below 690 K, and FCC, the stable allotropic modification at higher temperatures. With increase of pH, HCP is the only structure present and the texture of the deposits depends mainly on solution pH [18]. The prevailing orientations and their stability with respect to the operative conditions are characterized in detail for both sulfate [18] and chloride based electrolytes [19]. Cohen-Hyams et al. showed that the structure of electrodeposited Co depends significantly on the level of the overpotential [20]. When electrodeposition is performed far from equilibrium conditions, i.e. at higher overpotentials, FCC Co is deposited while at lower overpotentials HCP Co is formed with a lower rate of hydrogen evolution.

In the present paper, the composition, the morphology, and the microstructure of Ni–Co powders galvanostatically deposited on the Cu substrates are investigated as well as their thermal stability and structural changes in the temperature range from room temperature to 823 K.

2. Experimental procedure

Ni–Co alloys of different chemical compositions were prepared by electrochemical deposition from nickel and cobalt sulfate and ammonium chloride in ammonia based electrolytes containing Ni^{2+}/Co^{2+} concentration ratios of 4, 1 and 0.25 at pH 10 in a glass cell with a volume of 1.0 dm^3 at a temperature of 298 ± 1 K. The total concentration of $NiSO_4 + CoSO_4$ was 0.12 mol dm^{-3}. Electrodeposited Cu with a 1.0 cm^2 surface area and 0.2 cm thickness used as working electrodes were placed in the center of the cell. A Ti plate anode covered with RuO_2/TiO_2 (10 cm^2 geometric area) was placed close and parallel to the Cu plate. The electrodeposition of the powder was accomplished with a constant current in the range 40–00 mA cm^{-2}.

The surface morphology was analyzed with a scanning electron microscope (SEM) with field emission gun (XL 30 ESEM-FEG, FEI, NL) equipped with an energy dispersive X-ray spectrometer system (EDX) used for alloy composition analyses. The 3D reconstruction of the specimen surface was characterized using MeX software from Alicona (A). It enables a 3D analysis to be made directly from the digital images, yielding profile and roughness measurements and also area analysis as well as volumetric measurements.

X-ray powder diffraction (XRD) analysis was carried out using a MPD diffractometer (Philips) with Cu Kα radiation (40 kV/30 mA). The samples were analyzed in Bragg–Brentano geometry by means of step-scan mode in the range from 30° to 110° in 2θ with a step size of 0.03° and a counting time of 1.15 s/step. The XRD data were evaluated by means of the Rietveld refinement software package TOPAS (Bruker AXS, Germany). Values of the lattice cell parameters, crystallite size and the compositions of the samples were calculated. In addition, it was attempted to indicate values of the microstress, but the resulting values were below the error threshold for the samples. Therefore, this parameter was not usually refined. The progress of the refinement was checked by monitoring the goodness of fit parameter. In order to study the structural transformations induced by heating the samples of the alloy were annealed in sealed evacuated quartz tubes at selected temperatures for 30 min, water quenched and than analyzed by XRD.

Differential scanning calorimetry (DSC) measurements were performed with 10 mg samples using a DSC-204 C (Netzsch, D) in the temperature range of 298–823 K in an argon atmosphere with a heating rate of 20 K min^{-1}. Two heating runs were employed to obtain a baseline: the first heating run was with an as-prepared sample and the second heating run was conducted after cooling the sample to ambient temperature [21,22].

3. Results and discussion

In our experiments it was possible to obtain a defined amount of Ni–Co alloy only at current densities >40 mA cm^{-2} at the working electrode. However, in all bath compositions at current densities <65 mA cm^{-2}, compact deposits were obtained. For higher current densities (>150 mA cm^{-2}), the deposits were in the form of powders that could be easily removed from the electrode surface. It should be mentioned that for higher current densities, hydrogen evolution was quite intensive, providing conditions in which some amount of the powder drops into the cell.

(a) *Morphology of nanocrystalline deposits obtained from different bath compositions*

Fig. 1 presents SEM micrographs (micrographs (a)–(c)) of the alloys, electrodeposited from electrolytes with three different Ni^{2+}/Co^{2+} concentration ratios (4, 1, 0.25, respectively) at a current density of 65 mA cm^{-2}. The corresponding 3D SEM reconstructions of the surfaces are shown in Fig. 2. The deposit with the highest content of Ni^{2+} in the electrolyte (micrographs (a)) exhibits a cauliflower-like structure, consisting of small particles with an average radius <500 nm, surrounded by diffusion zones. The deposition took place in an spherically symmetrical pattern. For the ratio of $Ni^{2+}/Co^{2+} = 1$ (micrographs (b)), the morphology of the deposit is different and the cauliflower-like particles exhibit a platelet structure (Fig. 1(b)). Finally, the particles deposited from the electrolyte with the highest relative content of Co^{2+} (micrographs (c)) show a platelet structure with a preferred orientation and a size of the platelets in the μm range.

The quantitative 3D dataset for Fig. 2 was calculated from two stereoscopic images obtained by tilting the sample stage in the ESEM at the eucentric point at an angle of 5°. The calculated roughness parameters are shown in Table 1.

Concentration ratios $Ni^{2+}/Co^{2+} = 4$ and 0.25 led to surfaces with similar roughness values in spite of their different morphologies (Fig. 1(a) and (c)). In the case of $Ni^{2+}/Co^{2+} = 1$, the roughness of the deposit is about 3 times higher than that observed for the specimens obtained from the electrolytes with ratios of 4 or 0.25. Also the active surface (RS) increases in comparison with the specimens with ratios of 4 or 0.25. An increase in the current density results in a decrease in roughness since at higher current densities the number of crystal nuclei on the surface in enhanced. The larger the nucleation rate, the smaller the grain size is, leading to the formation of smooth deposits when the grain size ≤10 nm (confirmed by X-ray diffraction analysis).

(b) *Chemical composition of nanocrystalline deposits*

The chemical compositions of the galvanostatically deposited alloys as determined by EDX analysis of alloy samples with 10 μm^2 surfaces with an error of ±2% are summarized in Table 2.

According to the EDX results, an increase in current density leads to an increase in the Ni content of the deposits. At a current density of 65 mA cm^{-2}, the content of cobalt in the alloy is always higher than in the electrolyte as a consequence of the lower overpotential for the Co^{2+} reduction compared to Ni^{2+}.

The deposits (alloys 3, 4 and 5 in Table 2) obtained from an electrolyte with a concentration ratio $Ni^{2+}/Co^{2+} = 1$ for selected

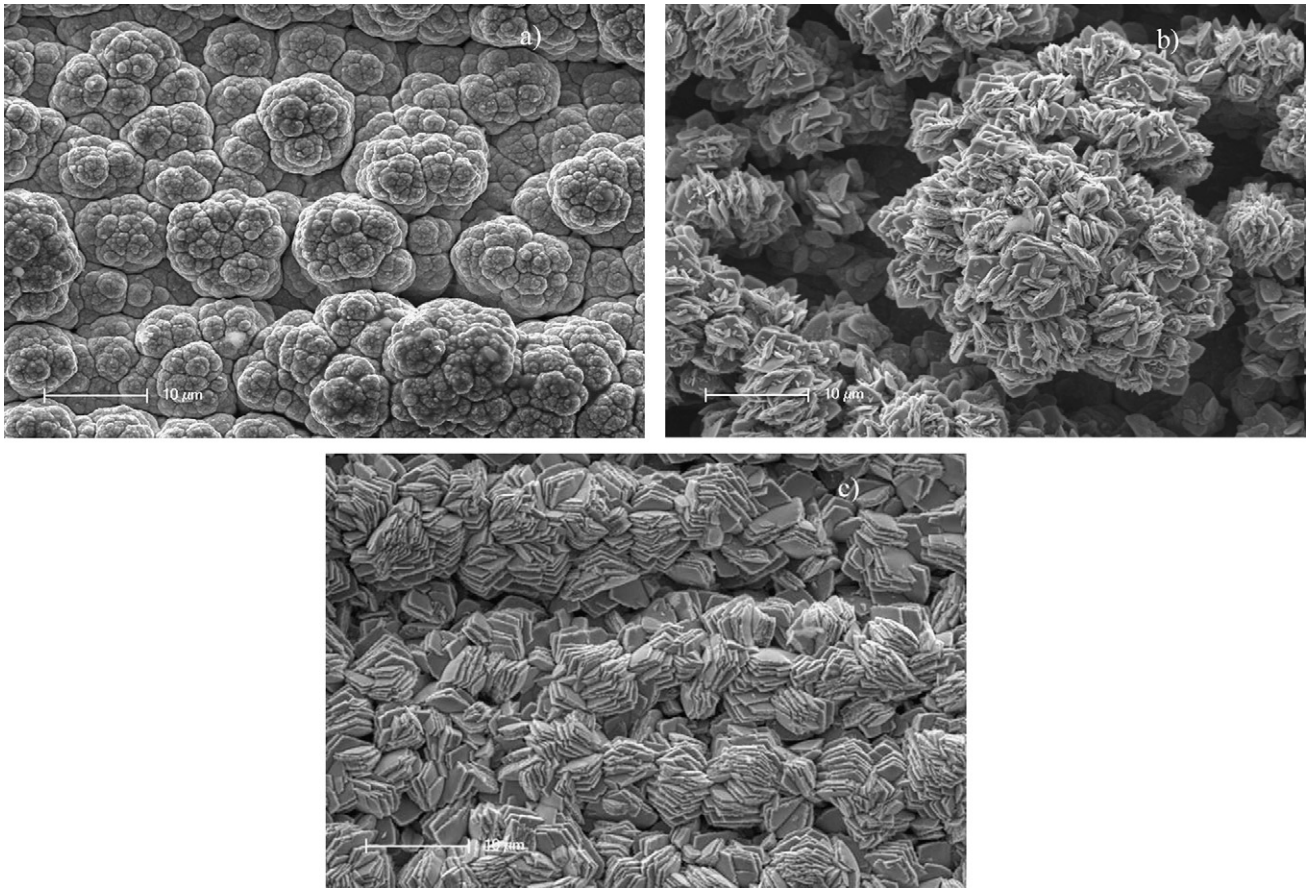

Fig. 1. SEM micrographs of Ni–Co deposits galvanostatically prepared from the electrolyte with different Ni^{2+}/Co^{2+} ratios: (a) 4, (b) 1, and (c) 0.25, at a current density 65 mA cm^{-2}.

current densities exhibit different compositions as well as structures. Increasing the current density shifts the ratio of nickel and cobalt in the alloys closer to the value of the concentration of the corresponding ions in electrolyte. The phenomenon of anomalous co-deposition (characteristic for the electrodeposition of iron group metals) is very pronounced in the production of compact deposits. However, in the case of powder deposition, anomalous co-deposition is much less pronounced, hence the composition of the alloy powder deposited at high current density is almost similar to the concentration of the metal ions in the electrolyte (alloy 5).

(c) *Structure of the Ni–Co nanocrystalline deposits*

The crystal structure, particle shape and size of the electrochemically obtained nickel–cobalt alloy deposits depend considerably on current density according to the SEM and X-ray diffraction analysis (Fig. 3). Mean grain sizes and lattice parameters were calculated from the peak broadening using the Scherrer equation with the Rietveld refinement method [23]. Powder particles obtained with geometric size varying from 1 μm to about 10 μm were composed of fine nanograined crystallites (cf. Table 3). Crystal structure and composition of the deposits obey the phase diagram [24].

As can be seen from the results (Fig. 3, Table 3), a deposit obtained from an electrolyte with a Ni^{2+}/Co^{2+} concentration ratio of 4 (alloy 1) consists of the α-Ni phase with a face-centered cubic lattice (FCC phase, space group *Fm*3*m*, *a* = 3.524 Å, JCPDS 00-004-0850). The diffraction peaks of Cu with low intensity result from the substrate material. The mean grain size in the FCC phase was 13 ± 2 nm. The alloy electrodeposited at the same current density with the ratio $Ni^{2+}/Co^{2+} = 0.25$ (alloy 2) consists of the ε-Co phase with a hexagonal-close packed lattice (HCP phase, space group *P*63/*mmc*, *a* = 2.506 Å, *c* = 4.069 Å, JCPDS 01-071-4239). With increasing Co content in the alloys (Table 3), the mean grain size increases and ranges from 13 ± 2 to 19 ± 3 nm for the FCC phase and from 15 ± 2 nm to 20 ± 3 nm for the HCP phase. The diffraction patterns of alloys deposited at relatively low current density for powder formation (65 mA cm^{-2}) show a strong texture. In particular, the texture for alloy 2 in planes (1 1 0) and (1 0 0) is an indication that the majority of grains are oriented with their close packed planes parallel to the surface, as it was shown in the SEM micrograph (Fig. 1(c)).

A detailed Rietveld's analysis revealed that Ni–Co alloys deposited from an electrolyte with the ratio $Ni^{2+}/Co^{2+} = 1$ at different current densities (alloys 3–5) are composed of solid solutions of both the cubic FCC phase and the HCP phase. This situation occurs due to the mutual miscibility of Ni and Co in the range of concentration in the deposits (Table 2). An increase in current density leads to an increase in the volume fraction of the FCC phase in the solid solution as well as the formation of a significant percentage of an amorphous phase.

An analysis of the diffractograms of the powdered alloys electrodeposited from the same electrolyte at different current densities, 65 mA cm^{-2} (alloy 3), 220 mA cm^{-2} (alloy 4) and 400 mA cm^{-2} (alloy 5), shows that the decrease of the current density results in pronounced crystallization and an increase in the size of crystallites as well as a higher volume fraction of the HCP phase. Furthermore, it can be seen that the cell volume of the alloys (alloys 3–5) increases slightly with increasing current density. Alloy 1 (rich in Ni) and alloy 2 (rich in Co) exhibit cell

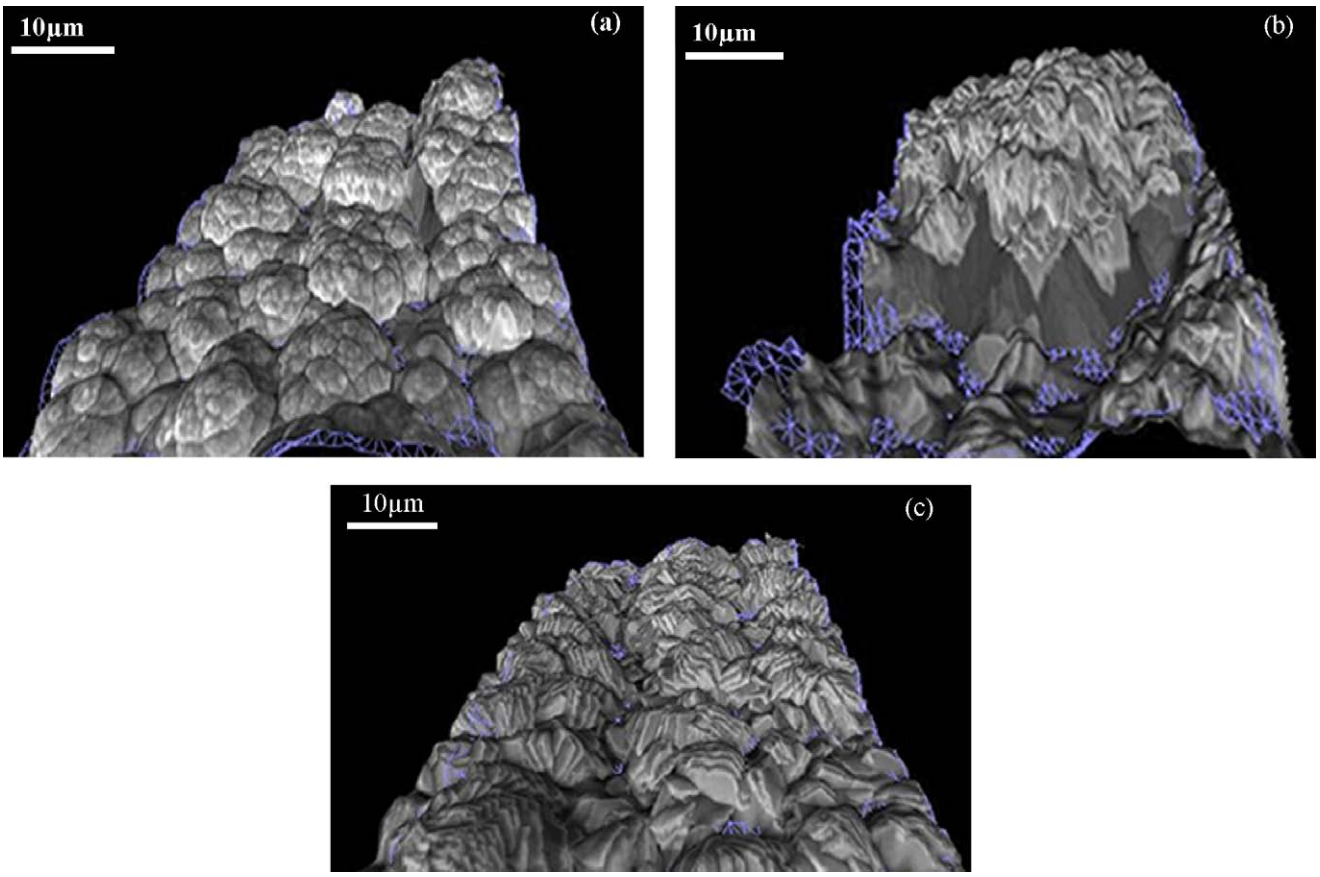

Fig. 2. 3D SEM reconstructions of the surfaces of Ni–Co deposits galvanostatically prepared from the electrolyte with different Ni^{2+}/Co^{2+} ratio: (a) 4, (b) 1, and (c) 0.25, at a current density 65 mA cm^{-2}.

volumes comparable to the theoretical values of Ni (43.8 Å^3) and Co (22.1 Å^3).

At lower current densities, the volume fraction of the Co in the deposit exists only as a single HCP phase; whereas with increasing current density the volume fraction of Co of the HCP Co is reduced down to 3%. Beside an amorphous content of 8–15% (Fig. 1), the rest of the Co forms a solid solution within the Ni FCC phase, resulting in an increase in the cell volume (see Table 3). The amorphous phase content was estimated by determination of the integral area of the broad diffuse diffraction halo which cannot be assigned to distinct diffraction maxima correlated with crystalline phases and comparing it with samples without amorphous phase.

(d) *Thermal stability of nanocrystalline deposits*

The thermal stability of alloys (prepared as powders from electrolytes with concentration ratios of for $Ni^{2+}/Co^{2+} = 4$ (alloy 1) and $Ni^{2+}/Co^{2+} = 0.25$ (alloy 2) at a current density of 65 mA cm^{-2} was characterized by DSC analysis (temperature range from room temperature to 823 K) as well as by X-ray diffraction and SEM methods. Because the intercrystalline volume represents a region of stored excess energy with respect to the bulk of a grain, there is a significant driving force for grain growth in nanocrystalline materials during heating. The structure of nanoscaled materials are thus thermodynamically unstable and show a strong tendency for structural changes under annealing [25] or even at room temperature [26]. These changes typically affect the density of crystalline defects, grain size, crystallographic orientation and grain boundary structure [27]. The enthalpy release due to annealing of the nanocrystalline structure can be directly measured by DSC.

Table 1
Roughness parameters of alloys deposited from electrolytes with different Ni^{2+}/Co^{2+} concentration ratios and current densities (Ra: mean roughness; Rz: difference between the highest and the lowest point in the picture of a given scan; RS: active surface, ratio of the real surface including topography to a projected surface of the measurements in a rectangle with dimensions of 23 μm × 15 μm).

Ni^{2+}:Co^{2+} concentration ratio	Current density (mA cm^{-2})	Ra (μm)	Rz (μm)	RS (μm^2)
4:1	65	1.0	4.7	1.64
1:1	65	3.0	13.1	1.98
1:1	220	1.1	5.2	1.38
1:1	400	1.0	6.5	1.62
1:4	65	0.7	4.7	1.64

3.1. Thermal stability of alloy 1

The thermal behavior of the Ni–Co powder of electrolyte ratio ($Ni^{2+}/Co^{2+} = 4$, $j = 65$ mA cm^{-2} – alloy 1) is depicted in a DSC curve, Fig. 4. The presence of two complex shaped exothermic peaks in the DSC curve indicates a stepwise process of the structural relaxation

Table 2
Chemical composition of the Ni–Co alloy deposits galvanostatically prepared from the electrolytes with different Ni^{2+}/Co^{2+} ratios and at different current densities.

	Alloy 1	Alloy 2	Alloy 3	Alloy 4	Alloy 5
Ni^{2+}/Co^{2+} ratio in the electrolyte	4	0.25	1	1	1
Current density (mA cm^{-2})	65	65	65	220	400
Ni content in alloy (at%)	80	5.5	33	40	43
Co content in alloy (at%)	20	94.5	67	60	57

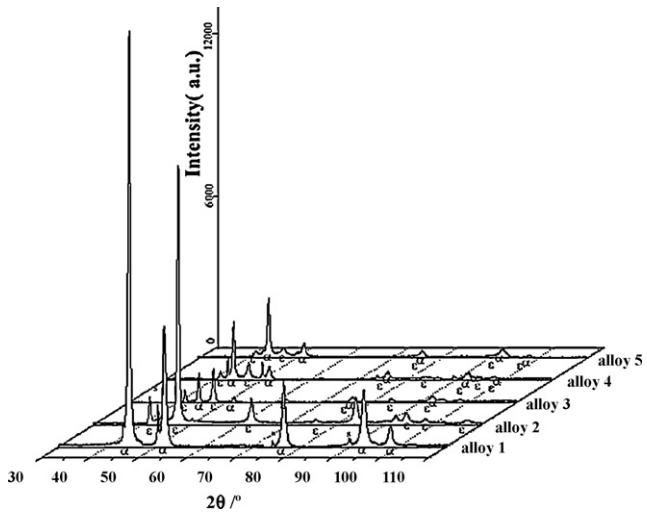

Fig. 3. X-ray diffraction patterns of Ni–Co deposits, experimental details as indicated in Table 2 (α – reflections attributed to the FCC Ni; ε – reflections attributed to the HCP Co; S – reflection attributed to the Cu substrate).

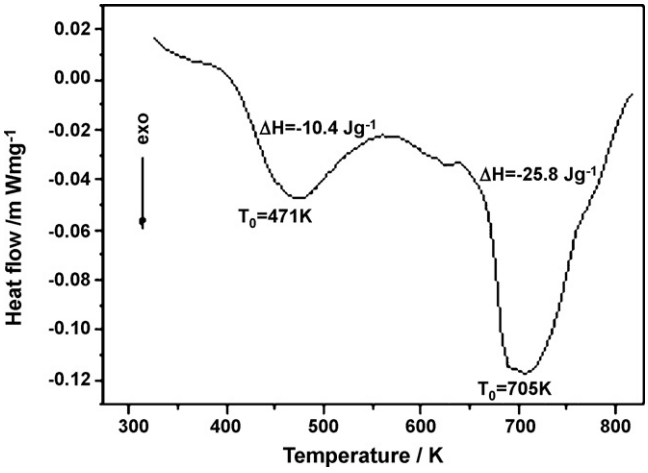

Fig. 4. DSC of the Ni–Co powder deposit prepared from the electrolyte with concentration ratio $Ni^{2+}/Co^{2+} = 4$ at a current density 65 mA cm^{-2} (alloy 1), heating rate 20 K min^{-1}.

and grain growth of the alloy powder in the temperature range of 393–823 K. The heat release associated with structural relaxation in the temperature range 393–573 K was $\Delta H = -10.4\,J\,g^{-1}$ and for further structural change in the temperature range 653–803 K the associated heat release was $\Delta H = -25.8\,J\,g^{-1}$.

Structural changes in Ni–Co deposits (alloy 1) induced by annealing at 523, 623 and 823 K are shown in the XRD pattern

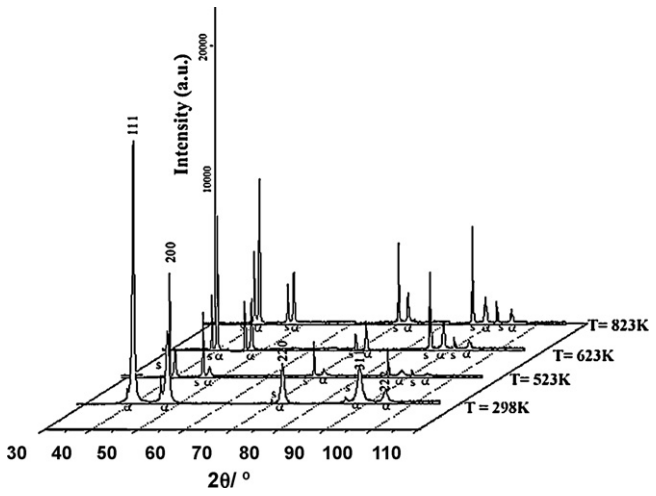

Fig. 5. XRD patterns of as-prepared alloy 1 deposited on Cu substrates and annealed samples at different temperatures. Experimental details are indicated in Table 2.

(Fig. 5). Rietveld refinement analysis (Table 4) shows only grain growth. No reflections related to cobalt or nickel oxides were detectable.

As found in many studies on the thermal stability of nanocrystalline materials [7–9,28], the Ni–Co alloy powder exhibits a quasi-nucleation growth-process during heating. When nanocrystalline deposits are brought to an elevated temperature, the nanometer-sized crystallites in the deposits start to grow in a random, non-uniform way and some of the existing nanocrystallites appear as nuclei and preferentially start to grow at the expense of the surrounding nanocrystalline matrix. With increasing temperature, the grains become larger and the lattice parameters of the FCC phase display only minor changes (Table 4). The pattern of the α phase at the temperatures higher as 523 K with respect to peak position and intensity remains unchanged, but the electrodeposited Cu substrate exhibits thermally induced restructuring, indicated by a significant change in the diffraction pattern (decreasing of the 1 1 1 reflection intensity and increasing of the 2 2 0 and 3 1 1 reflections).

A typical SEM micrograph of an alloy obtained upon annealing at 823 K is shown in Fig. 6. The composition as well as the structure of the deposit was attained with no significant change in the particle size as compared to the SEM image of an as-deposited sample shown in Fig. 1(a).

3.2. Thermal stability of alloy 2

The thermal behavior of the Ni–Co powder of alloy 2 (electrolyte ratio $Ni^{2+}/Co^{2+} = 0.25$, $j = 65$ mA cm^{-2}) is depicted in a DSC curve, Fig. 7. The presence of a broad asymmetric exothermic peak indicates a stepwise process of the structural relaxation and phase

Table 3
Phase composition, grain size and cell parameters of the Ni–Co deposits; experimental details as indicated in Table 2.

Alloy	Crystal structure/content (%)	Grain size (nm)	Lattice parameter (Å)		Cell volume (Å^3)
			a	*c*	
Alloy 1	FCC/100	13 ± 2	3.5259(3)		43.833(9)
Alloy 2	HCP/100	20 ± 3	2.5057(2)	4.0690(4)	22.126(4)
Alloy 3	FCC/28	19 ± 3	3.5291(2)		43.955(4)
	HCP/72	15 ± 2	2.5053(2)	4.0717(3)	22.127(4)
Alloy 4	FCC/70	13 ± 2	3.5296(3)		43.971(9)
	HCP/22 amorphous phase/8	11 ± 2	2.4987(4)	4.0767(2)	22.043(8)
Alloy 5	FCC/82	11 ± 2	3.5329(3)		44.096(9)
	HCP/3 amorphous phase/15	10 ± 2	2.4947(5)	4.1005(3)	22.100(5)

Table 4
Phase composition and grain sizes of the as-deposited and annealed Ni–Co deposits (alloy 1 – prepared from the electrolyte with concentration ratio $Ni^{2+}/Co^{2+} = 4$ at a current density 65 mA cm^{-2}).

Alloy	Crystal structure	Grain size (nm)	Lattice parameter a (Å)	Cell volume (Å^3)
Alloy 1 as-prepared at 298 K	FCC	13 ± 2	3.5259(3)	43.833(9)
Alloy 1 annealed at 523 K	FCC	20 ± 3	3.5274(2)	43.891(7)
Alloy 1 annealed at 623 K	FCC	47 ± 4	3.5270(2)	43.876(6)
Alloy 1 annealed at 823 K	FCC	57 ± 6	3.5305(8)	44.004(3)

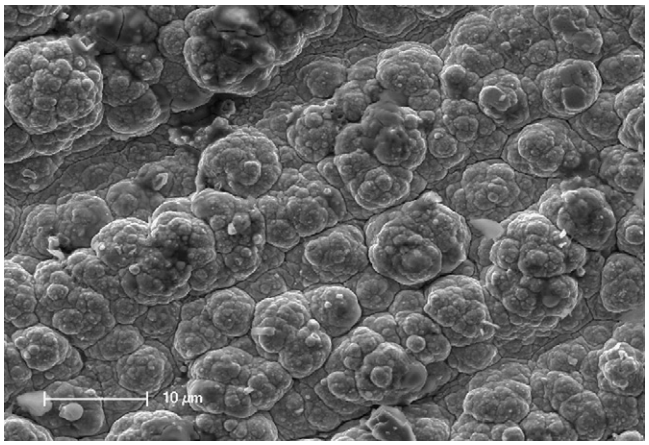

Fig. 6. SEM micrograph of Ni–Co deposit upon annealing at 823 K (alloy 1 prepared from the electrolyte with concentration ratio $Ni^{2+}/Co^{2+} = 4$ at a current density 65 mA cm^{-2}; magnification 2000× (SE, accelerating voltage 10 kV).

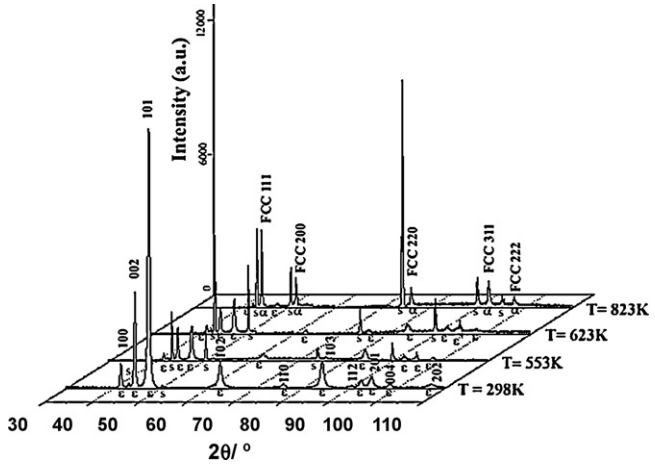

Fig. 8. XRD patterns of as-prepared alloy 2 deposited on Cu substrates and annealed samples at different temperatures. Experimental details are indicated in Table 2.

transformation of the alloy in the temperature range 573–823 K. The first exothermic feature in the temperature range 553–573 K can be attributed to structural relaxation processes of the HCP phase. During grain growth, as the system moves from the condition of an as-deposited nanocrystalline sample of higher excess free energy to the condition of the annealed sample exhibiting lower excess of free energy, there is an enthalpy release of $\Delta H = -190.6\,J\,g^{-1}$ giving a measure of the thermal stability of the sample with respect to the phase transformation HCP → FCC.

Structural changes in Ni–Co deposits (alloy 2) induced by annealing at 553, 623 and 823 K are shown in the XRD pattern (Fig. 8).

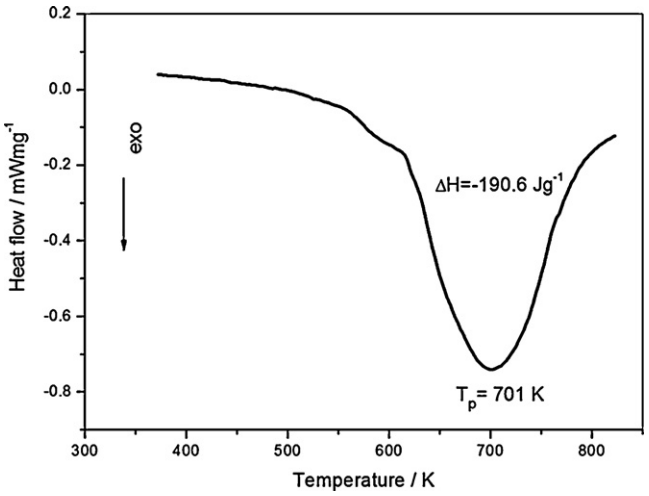

Fig. 7. DSC of the Ni–Co powder deposit prepared from the electrolyte with concentration ratio $Ni^{2+}/Co^{2+} = 0.25$ at a current density 65 mA cm^{-2} (alloy 2); heating rate 20 K min^{-1}.

The XRD of the as-deposited samples show the presence of only the HCP phase with a mean grain size of 20 nm, Fig. 3. According to the X-ray diffraction analysis of annealed samples, the volume fraction of the low temperature HCP phase is continuously reduced upon annealing.

The mean grain size of the FCC phase increases up to 50 nm, while the mean grain size of the HCP phase decreases down to 7 nm (Table 5). Annealing at temperatures of 553 and 623 K caused only slight difference in grain size and lattice constant (Table 5). However, annealing at a temperature of 823 K generated grain size and lattice constant changes due to the austenitic allotropic phase transformation (HCP → FCC). At 823 K, the high temperature phase FCC appears, and being retained after cooling at room temperature. The sample annealed at 823 K shows a higher value of the lattice parameter ($a = 3.4567$ Å). The variation is most likely related with changes in the chemical composition (i.e. Co/Ni ratio) in the FCC phase. As in the case of alloy 1, the electrodeposited substrate exhibits also structural changes, especially after annealing at a temperature of 823 K the intensity of the 2 2 0 reflection increases significantly, indicating texture development.

The austenitic phase transformation temperature is a function of heating rate [29] and in polycrystalline Co occurs at 695 K. Considering the chemical composition of an alloy with 94.5% of Co in the nanocrystalline deposit (cf. Table 3), based on the phase diagram [24] it can be assumed that the phase transformation occurred at about the same temperature. DSC results confirmed this assumption since a heat released associated with a phase transformation has a maximum at 701 K. The volume fraction of the FCC phase retained upon cooling to room temperature was over 70%.

SEM micrographs of annealed alloy 2 are shown in Fig. 9. The platelet structure is preserved; however, the top of the particles consists of the platelets with reduced size compared to the as-deposited sample (Fig. 1(c)).

Table 5
Phase composition and grain sizes of the as-deposited and annealed Ni–Co deposits (alloy 2 – prepared from the electrolyte with concentration ratio $Ni^{2+}/Co^{2+} = 0.25$ at a current density 65 mA cm^{-2}).

Alloy	Crystal structure	Grain size (nm)	Lattice parameter (Å)		Cell volume (Å^3)
			a	*c*	
Alloy 2 as-prepared at 298 K	HCP	20 ± 3	2.5057(2)	4.0690(4)	22.126(5)
Alloy 2 annealed at 553 K	HCP	21 ± 3	2.5071(2)	4.0706(3)	22.159(4)
Alloy 2 annealed at 623 K	HCP	19 ± 3	2.5079(2)	4.0714(4)	22.177(4)
Alloy 2 annealed at 823 K	FCC	50 ± 5	3.5467(1)		44.616(7)
	HCP	7 ± 2	2.4790(4)	4.257(2)	22.660(1)

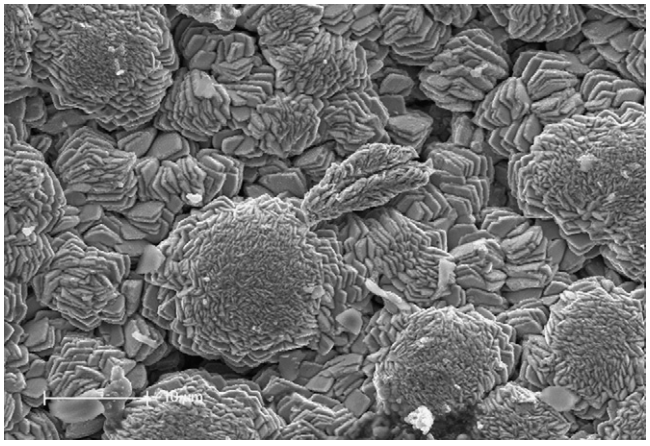

Fig. 9. SEM micrograph of Ni–Co deposit upon annealing at 823 K (alloy 2 prepared from the electrolyte with concentration ratio $Ni^{2+}/Co^{2+} = 0.25$ at a current density 65 mA cm^{-2}); magnification 2000× (SE, accelerating voltage 10 kV).

4. Conclusions

The structure and morphology of the Ni–Co alloy powders galvanostatically deposited from ammonium nickel and cobalt sulfate solutions depend significantly on the deposition current density as well as the bath composition. The FCC phase is the predominant phase in the alloy deposit obtained from the electrolytes with a ratio $Ni^{2+}/Co^{2+} = 4$. An increase in the volume fraction of the HCP phase in the nanocrystalline deposits is caused by an increase in the Co^{2+} ion concentration in the bath and by a decrease of the deposition current density, whereas an increase of the current density and a decrease of the Co^{2+} ion concentration in the bath yield finer grain deposits. An increase of the deposition current density in electrolytes with a ratio $Ni^{2+}/Co^{2+} = 1$ leads to a decrease of the volume fraction of the HCP phase in the obtained deposits. Under heating, a significant thermal effect in nanostructured Ni–Co alloy powder deposits has been observed. On the whole, a heat release in the deposit obtained from electrolytes with a ratio $Ni^{2+}/Co^{2+} = 0.25$ is caused by both, the phase transformation and grain growth. The heat release associated with the phase transformation (HCP → FCC) has a maximum at 701 K. Annealing at 823 K results in the appearance of the high temperature phase FCC being retained at room temperature.

Acknowledgments

This research was supported by the research project "Bulk Nanostructured Materials" within the research focus "Material Science" of the University of Vienna. The investigation was partially supported by the Ministry of Science and Environmental Protection of Serbia, under Project 142025 and within the K plus programme at CEST by the Austrian Research Promotion Agency (FFG) and the government of Lower Austria.

LR is grateful for the support by the I.K. "Experimental Materials Science – Nanostructured Materials", a college for PhD students at the University of Vienna.

References

[1] H. Gleiter, Nanocrystalline materials, Prog. Mater. Sci. 33 (1989) 223.
[2] R.P. Andres, R.S. Averback, W.L. Brown, L.E. Brus, W.A. Goddard III, S.G. Kaldor, J. Mater. Res. 4 (1989) 704.
[3] M.A. Meyers, A. Mishra, D.J. Benson, Prog. Mater. Sci. 51 (2004) 427.
[4] U. Erb, Nanostruct. Mater. 6 (1995) 533.
[5] N.V. Myung, K. Nobe, J. Electrochem. Soc. 148 (2001) 136.
[6] D.-Y. Park, K.S. Park, J.M. Ko, D.-H. Cho, S.H. Lim, W.Y. Kim, B.Y. Yoo, N.V. Myung, J. Electrochem. Soc. 153 (2006) 814.
[7] G.D. Hibbard, K.T. Aust, U. Erb, Mater. Sci. Eng. A 433 (2006) 195.
[8] G. Hibbard, U. Erb, K.T. Aust, U. Klement, G. Palumbo, Mater. Sci. Forum 386–388 (2002) 387.
[9] G. Wilde, P. Bunzel, H. Rösner, J. Weismüller, J. Alloys Compd. 434–435 (2007) 286.
[10] K.I. Popov, M.G. Pavlović, Electrodeposition of metal powders with controlled particle grain size and morphology, in: R.E. White, B.E. Conway, J.O'M. Bockris (Eds.), Modern Aspects of Electrochemistry, vol. 24, Plenum Press, New York, 1993 (Chapter 6).
[11] K.I. Popov, S.S. Djokić, B.N. Grgur, Fundamental Aspects of Electrometallurgy, Kluwer Academic Press, New York, USA, 2002.
[12] A. Calusaru, Electrodeposition of Powders from Solutions, Elsevier, New York, USA, 1979.
[13] A. Maričić, M. Spasojević, L. Rafailović, V. Milovanović, L. Ribić-Zelenović, Mater. Sci. Forum 453–454 (2004) 411.
[14] L. Ribić-Zelenović, L. Rafailović, M. Spasojević, A. Maričić, Sci. Sinter. 38 (2006) 145.
[15] L. Ribić-Zelenović, L. Rafailović, M. Spasojević, A. Maričić, Phys. B: Conden. Matter 403 (2008) 2148.
[16] A. Bianco, G. Gusmano, R. Montanari, G. Montesperelli, E. Traversa, Thermochim. Acta 269–270 (1995) 117.
[17] A. Vicenzo, P.L. Cavallotti, Electrochim. Acta 49 (2004) 4079.
[18] S. Armyanov, S. Vitkova, Surf. Technol. 7 (1978) 319.
[19] J. Scoyer, R. Winand, Surf. Technol. 5 (1977) 169.
[20] T. Cohen-Hyams, W.D. Kaplan, J. Yahalom, Electrochem. Solid-State Lett. 5 (2002) 75.
[21] L.C. Chen, F. Spaepen, J. Appl. Phys. 69 (1991) 679.
[22] F.O. Méar, B. Lenk, Y. Zhang, A.L. Greer, Scr. Mater. 59 (2008) 1243.
[23] H. Rietveld, J. Appl. Crystallogr. 2 (1969) 65.
[24] T.B. Massalski, Binary Alloy Phase Diagrams, ASM International, Materials Park, OH, USA, 1991.
[25] F. Czerwinski, A. Zielinska-Lipiec, J.A. Szpunar, Acta Mater. 47 (1999) 2553.
[26] B. Bozzini, G. Giovannelli, P.L. Cavallotti, J. Appl. Electrochem. 30 (2000) 591.
[27] L. Peraldo Bicelli, B. Bozzini, C. Mele, L. D'Urzo, Int. J. Electrochem. Sci. 3 (2008) 356.
[28] N. Wang, Z. Wang, K.T. Aust, U. Erb, Acta Mater. 45 (1997) 1655.
[29] G. Hibbard, K.T. Aust, G. Palumbo, U. Erb, Scr. Mater. 44 (2001) 513.